IOSR Journal of Mechanical and Civil Engineering (IOSR-JMCE)
e-ISSN: 2278-1684,p-ISSN: 2320-334X, Volume 12, Issue 6 Ver. V (Nov. - Dec. 2015), PP 53-65
www.iosrjournals.org

Influence of phase transformation on the work hardening characteristics of Pb-(1-3)wt.%Sb alloys

Gh. Mohammed[1], S. El-Gamal*[1], A. S. Mahmoud[2], R. H. Nada[2] and A.M. Abd El-Khalek[2]

[1] *Physics Department, Faculty of Science, Northern Borders University, Arar, 91431, KSA, permanent address; Physics Department, Faculty of Education, Ain Shams University, Cairo, 11747, Egypt.*
[2]*Physics Department, Faculty of Education, Ain Shams University, Cairo, 11747, Egypt*
**Corresponding author. Tel.: 0966 567414468. E-mail address: samyelgamal@gmail.com*

Abstract: *This study focuses on the effect of phase transformation on the work hardening characteristics of Pb-(1-3)wt.%Sb alloys either quenched (type I) or slowly cooled samples (type II) at different ageing temperature (T_a). Three work hardening characteristics were studied which are; the coefficient of work hardening χ_p, yield stress σ_y and fracture stress σ_f. It was found that; these parameters of both types of samples decrease with increasing T_a, showing two stages around the transformation temperature which changes with the Sb addition and equal to 453 K for 1wt.%Sb, 483 K for 2wt.%Sb and 513 K for 3wt.%Sb. The values of these parameters of type I samples were higher than type II samples. The fracture strain ε_f, the strain at the fracture point, increases with increasing T_a showing two stages also. The dislocation slip distance, L, increases as T_a increases. The magnitude of the variation of all these parameters point to two fracture mechanisms activated with 0.11 and 0.39 eV for 1wt.%Sb, 0.15 and 0.49 eV for 2wt.%Sb, 0.20 and 0.65 eV for 3wt.%Sb for type I samples and equal 0.21 and 0.52 eV for 1wt.%Sb, 0.17 and 0.56 eV for 2wt.%Sb, 0.16 and 0.63 eV for 3wt.%Sb for type II for both first and second stages, respectively. The microstructure of the samples under investigation has been examined after stress-strain measurements by scanning electron microscope.*

Keywords: *Work hardening characteristics, Ageing temperature, Pb-Sb alloys, Mechanical characterization*

I. Introduction

Lead is very soft and ductile so it is normally used commercially as lead alloys [1]. Lead alloys had become established by the end of the first half of the twentieth century [2]. Antimony, tin, arsenic, and calcium are the most common alloying elements [3]. The addition of Antimony, in particular, enhances the alloy hardness greatly and lowers the casting temperature and minimizes the contraction during freezing. Indeed, such addition plays a vital role in increasing the resistance to compressive impact and wear [4]. Also, it increases the conductive properties [5]. In fact, such addition produces a significant segregation at grain boundaries and a high concentration of alloying vacancies which should modify the viscous flow processes along the grain boundaries [6]. Antimony contents in lead-antimony alloys can range from 0.5 to 25%, but they are usually about 2-5% [1]. Lead- antimony alloys are considered as an important material in industrial applications for their use as the best stable material for battery grids in accumulator manufacturing [7, 8] because of the properties of Pb-Sb alloys, mentioned lately. It should be noted that, these alloys are very well hardened by continuous precipitation, whereas lead–tin alloys present a discontinuous precipitation with a weak hardening effect [9]. It is noted that, the choice of the suitable heat treatment plays an important role in enhancing the mechanical properties of the metallic materials to achieve more applications in industry and this topic attracts more and more investigators [10-15]. Pb-Sb alloy consists of Pb-rich phase and some amounts of Sb-rich phase this is according to its phase diagram [16]. It was reported that, Sb-rich phase has always formed at the boundaries of Pb-rich phase [7] and the solid solubility of Sb in Pb increases as the heating temperature increases up to transformation temperature. The process of ageing of the super-saturated solid solution of this alloy leads to the formation of more β-phase.

The thorough surveying of the literature has revealed that; some investigators were interested in studying the corrosion resistance and electrochemical behavior of the Pb-Sb alloys [2, 17] while others studied their structure and mechanical properties by changing the deformation temperature [18, 19] or with adding of tin [18]. As was noticed, little attention has been given to the topic of effect of ageing temperature (423-543 K) on the work hardening characteristics of Pb-(1-3)*wt.*%Sb alloys and this represents a gap. So the aim of the present work is to try to fill this gap.

II. Experimental procedure

2.1 Alloy preparation and heat treatment

Pb-(1-3)*wt.*%Sb alloys were prepared from high purity Pb and Sb (99.99%) by melting a mixture of the appropriate weights under vacuum in a high purity graphite crucible, in a high frequency induction furnace. The obtained ingot was homogenized at 553 K for 8 h then cold drawn into two forms; wires of diameter 0.6 mm and sheets of thickness 0.4 mm. Chemical analysis revealed that sample composition is very close to the alloy compositions required. The samples were divided into two parts, one of them were quenched in water at RT (type I) while the remaining (other) part were slowly cooled (type II). Ageing of the samples (wires and sheets) were performed in the temperature range; 423-483K, 453-513K and 483-543 K for Pb-1*wt.*%Sb, 2*wt.*%Sb and 3*wt.* %Sb alloys, respectively, with accuracy ±2 K, at an interval of 10 K and the time of ageing was 1 hr.

2.2 Measurements

2.2.1 Tensile test

One of the most important tests to investigate the material's mechanical properties is the tensile test. This test was performed using a computerized locally made tensile testing machine. More details about this machine were described elsewhere [20]. All samples were stretched with a constant strain rate of 1.2×10^{-3} s^{-1} at room temperature (300 K) up to fracture.

2.2.2 Microstructure examination

The microstructure of Pb-Sb alloys were investigated using scanning electron microscope (SEM) (JEOL, JSM-5400) and energy dispersive X-ray spectroscopy (EDS). Using different techniques helped us to investigate the microstructure precisely.

III. Results

3.1 Tensile properties

The engineering stress-strain curves at different T_a for both types of Pb-(1-3)*wt.*%Sb alloys are shown in Figs. (1-3). It was found that, the stress-strain curves vary with changing T_a for the both types of the samples. Figs. (4-6) show the dependence of the work hardening parameters (χ_p, σ_y and σ_f) on T_a. Where σ_y is called the yield stress, σ_f is the fracture stress and χ_p is the work-hardening coefficient, which could be calculated from the parabolic part of stress-strain curves (Figs. (1-3)) by using the following equation;

$$\chi_p = \left(\frac{\partial \sigma^2}{\partial \varepsilon}\right)_T \qquad (1)$$

It was found that, the three parameters decrease as the ageing temperature increases for the both types of the samples and such decrease occurred in two distinguished stages. The first one extends to temperatures up to 453 K for 1*wt.*% Sb, 483 K for 2*wt.*% Sb and 513 K for 3*wt.*% Sb and the second stage extends to a higher range above 453 K, 483 K and 513 K. The values of χ_p, σ_y and σ_f for samples of type I are higher than those of type II. The fracture strain ε_f (the strain corresponding to the fracture point in the stress-strain curves) as a function of T_a is shown in Fig. 7. It is clear that ε_f increases as the ageing temperatures increase and showing two stages for the two types of alloy samples. Also, the value of ε_f for type I samples were found to be less than type II at all the applied temperatures. The dislocation slip distance L is one of the important parameters in the field of tensile properties of materials [21]. Its values could be found by applying Mott's work hardening model [22]. The model predicts that the coefficient of work hardening χ_p is given by the equation:

$$\chi_p = \frac{G^2 b}{2\pi^2 L} \qquad (2)$$

where L is the distance slipped by the moving dislocation, G is the shear modulus for Pb alloy ($G=4.3\times10^4$ MPa), and b is the Burgers vector ($b = 3.5\times10^{-10}$ m) [23]. The dependence of L on T_a for both types of samples is depicted in figure 8. It is clear that, increasing T_a resulted in increasing L.

2-Structural properties

It is well known that, investigating the microstructure of different Pb-(1-3)*wt.*%Sb alloys plays a vital role in determining and predicting the mechanical response. In the present study, the evaluation of the microstructure changes due to the aging temperature under different conditions was performed by using SEM and EDS investigations.

Figure 9 shows SEM micrographs of the Pb-*2wt.*% Sb quenched samples (type I) aged for 1h at the temperatures 463,483 and 513K. As observed, there are two phases, dark phase and white phase, the white phase was detected to be Sb-rich phase embedded in dark phase, which is the Pb-matrix and this was confirmed by EDS investigation. Also, the Sb-rich phase in Pb-matrix decrease with increasing ageing temperature.

IV. Discussion

The stress-strain curves in the present work were considered as raw experimental data and hence it is more suitable to discuss the parameters extracted from these curves other than discussing the curves themselves. The decrease in χ_p, σ_y and σ_f in the first stage (see Figs. (4-6)) could be attributed to the amount of the second phase (β-phase or Sb-rich phase) and its corresponding diffusivity with the matrix (Pb) which controls the dislocation mobility at the inter-phase boundaries [24]. This continues until the transformation temperature, which is 453 K, 483 K and 513 K for 1, 2 and 3*wt*. % Sb respectively. But, in the second stage, i.e., above transformation temperature, the β-phase dissolves completely and disappears [25] and this result in an intensive decrease in the work hardening parameters which could be due to the relaxation of dislocations at the fronts of the pileups at grain boundaries [26]. This process might be associated with dislocation annihilation by increased thermal agitation [18]. The above explanation was confirmed by SEM micrographs (see Fig. 9) for the sample Pb 2*wt*.% Sb, as an example, at different ageing temperatures 463, 483 and 513 K. From these micrographs, the solubility of Sb-rich phase in Pb-matrix increases until the transformation temperature, 483 K, and after that the Sb-rich phase disappears.

On the other hand, ε_f increases as T_a increases (see Fig. 7) because in the first stage the solubility of Sb in Pb increases, so the motion of dislocations enhanced as a result of the decrease in the percent of Sb-rich phase. In the second stage the materials became more ductile due to the rearrangement of the dislocations [27].

The higher values of χ_p, σ_y and σ_f for type I samples compared with type II is due to the more tangling in dislocations occurred in type I samples because of the quenching process [28] which obstacle the movement of Sb-rich phase. But for type II samples the dislocation motion is easier.

The higher values of ε_f of the type II samples than type I (see Fig. 7) is due to the relaxation of alloy as a result of some degree of dislocation annihilation which accelerate the solubility of β-phase in the matrix, reduces the hardness and consequently increases the ductility, i.e., ε_f increases. For type I samples, ε_f is lower because the sample became harder due to the quenching process. Increasing the Sb content, the work hardening parameters increases while ε_f decreases this is because the addition of Sb hardens the alloy.

The increase in L as T_a increases (see Fig. 8) could be due to the relaxation of dislocation heads of the pileups at the phases existed in the Pb-matrix. This relaxation is accompanied by escaping of dislocations from these pileups by the cross-slipping process as a result of the thermal agitation. Finally, the dislocations will move through longer slip distances L.

The activation energies of the operating mechanisms in both types I and II are determined from the slopes of the straight lines of the relation between Ln (σ_f) and 1000/T as shown in Fig. 10 according to the Arrhenius's equation;

$$\sigma_f = A \exp. (Q/RT) \qquad (3)$$

where A is a constant, Q is the activation energy in eV and R is the gas constant. The values of the activation energies were represented in Table (1). It is clear that, the values of Q in type II samples are higher than that of type I. For all the samples, Q values in region II are higher. These values indicate that the operating mechanism may be a dislocation intersection [8, 29] and diffusion of Sb through Pb-Sb boundaries [8] in the low temperature range. While in the high temperature range, grain boundary sliding is the principal mechanism [7, 8].

V. Conclusion

The effect of phase transformation on the work hardening characteristics of Pb-(1-3)*wt*.%Sb alloys either quenched (type I) or slowly cooled samples(type II) at different ageing temperature (T_a) was studied. The coefficient of work hardening χ_p, yield stress σ_y and fracture stress σ_f were found. They decrease with increasing T_a in two stages around the transformation temperature. The transformation temperature changes with the addition of Sb and equal 453 K for 1*wt*.%Sb, 483 K for 2*wt*.%Sb and 513 K for 3*wt*.%Sb. The values of these parameters of the type I samples were higher than those of type II. The fracture strain ε_f, the strain at the fracture point, increases with increasing T_a showing two stages also. The dislocation slip distance, L, increases as T_a increases. The operating mechanism may be dislocation intersection and diffusion of Sb through Pb-Sb boundaries in the low temperature range and changed to the grain boundary sliding in the high temperature range.

References

[1] Davis J R, Alloying: Understanding the Basics, ASM International (2001)
[2] Ghasemi Z and Tizpa A, Int. J. Electrochem. Sci. 3 (2008) 727.
[3] Morrison R D and Murphy B L, Environmental Forensics: Contaminant Specific Guide, Academic Press (2005).
[4] Metikos-Hukovic M, Babic R and Brinic S, J Power Sources 64 (1997) 13.
[5] Laitinen T, Salmi K, Sundholm G, Monghova B, and Pavlova D, Electrochimica Acta 36(3-4), (1991) 605.
[6] Elsukova T F, Panin V E, Veselova D V and Veselov Yu G, Russian Phys J 30 (11) (1988) 923.
[7] Al-Ganainy G S, Mostafa M T and Nagy M R, Phys. Stat. Sol. A 165 (1998) 185.
[8] Al-Ganainy G S, Mostafa M T and Abd El-Salam F, Physica B 348 (2004) 242.

[9] Hilger J P, J. Power Sources 53 (1995) 45.
[10] El-Gamal S and Mohammed Gh, Radiat. Phys. Chem. 99 (2014) 68-73.
[11] El-Gamal S and Mohammed Gh, J Iron Steel Res Int, 23 (7) (2016), accepted to be published.
[12] Abdel-Hady E E, Ashry A, Ismail H, El-Gamal S, Appl. Surf. Sci. 252 (2006) 3297.
[13] El-Gamal S, Radiat. Phys. Chem. 90 (2013) 32.
[14] Saad G, Soliman H N, Fawzy A, Mohammed Gh, Arab J Nucl Sci Appl. 44 (2011) 313.
[15] Habib N, Mohammed Gh, Saad G, Fawzy A, Arab J Nucl Sci Appl. 41(1) (2008) 215.
[16] Hansen M, Constitution of binary alloys 2 ed., McGraw-Hill, London (1958)
[17] Ghasemi Z and Tizpa A, Int. J. Electrochem. Sci. 2 (2007) 700.
[18] Abd El-Khalek A M and Nada R H, Physica B 328 (2003) 393.
[19] Fawzy A, Awadallah A S M, Sobhy M, and Saad G, Physica B 355 (2005) 286.
[20] Saad G, Fayek S A, Fawzy A, Soliman H N and Mohammed Gh, Mat. Sci. Eng. A-Struct. 527 (2010) 904.
[21] Shaha S K, Czerwinski F, Chen D L and Kasprzak W, Mater Sci Tech 31(1) (2015) 63.
[22] Mott N F, Dislocations and Mechanical Properties of Crystals, Wiley, New York, (1957).
[23] Kittel C, Introduction to Solid State Physics, Wiley Eastern Ltd., New Delhi, (1984).
[24] Lukac P, Malygin G A and Vladimirova A G V, Czech. J. Phys. B 35(3) (1985) 318.
[25] El-Sayed M M, Abd El-Salam F, Abd El-Haseeb R and Nagy M R, Phys. Stat. Sol. A 144 (1994) 329.
[26] Soer W A, Interactions between dislocations and grain boundaries, PhD thesis series, 2006
[27] Reardon C, Metallurgy for the Non-Metallurgist 2ed, ASM International, (2011).
[28] Lim N S, Bang C W, Das S, Jin H W, Ayer R and Park C G, Met. Mater. Int. 18(1) (2012) 87.
[29] El-Sayed M M, Abd El-Salam F, Abd El-Haseeb R, Phys. Stat. Sol. A 147(2) (1995) 401.

Figure Captions

Fig. (1): Stress–strain curves of both types of Pb–1*wt.*%Sb alloy.
Fig. (2): Stress–strain curves of both types of Pb–2*wt.*%Sb alloy.
Fig. (3): Stress–strain curves of both types of Pb–3*wt.*%Sb alloy.
Fig. (4): The dependence of work-hardening coefficient, χ_p on the ageing temperature for both types of Pb–1-3*wt.*% Sb alloys.
Fig. (5): The dependence of yield stress, σ_y on the ageing temperature for both types of Pb–1-3*wt.*% Sb alloys
Fig. (6): The fracture stress, σ_f as a function of ageing temperature for both types of Pb–1-3*wt.*% Sb alloys
Fig. (7): The fracture strain, ε_f as a function of ageing temperature for both types of Pb–1-3*wt.*% Sb alloys
Fig. (8): Temperature dependence of slip distance, *L* for both types of Pb–1-3*wt.*% Sb alloys
Fig. (9): SEM micrographs of the quenched samples (2*wt.*% Sb) at different ageing temperatures
Fig. (10): The relation between Ln (σ_f) and 1000/T of both types of Pb–1-3*wt.*% Sb alloys
Table (1): The values of the activation energies for both types of Pb–1-3*wt.*% Sb alloys

	Region I		Region II	
	Type I	Type II	Type I	Type II
1 wt.% Sb	**0.11**	**0.12**	**0.39**	**0.52**
2 wt.% Sb	**0.15**	**0.17**	**0.49**	**0.56**
3 wt.% Sb	**0.20**	**0.16**	**0.65**	**0.63**

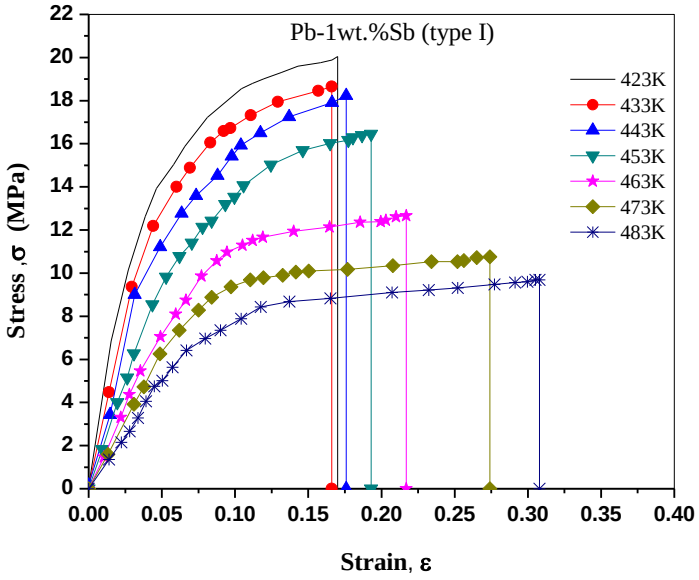

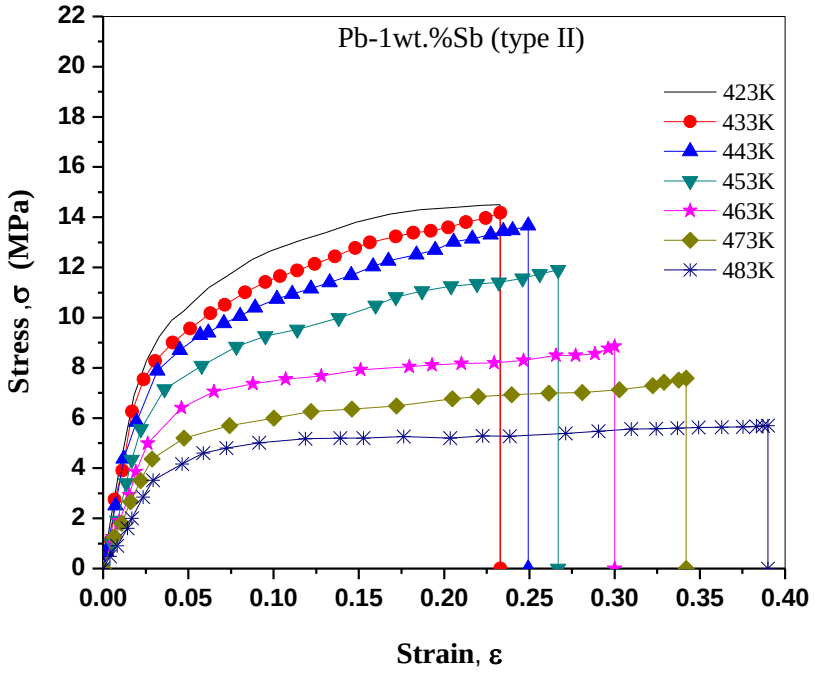

Fig. (1): Stress–strain curves of both types of Pb–1*wt*% Sb alloy.

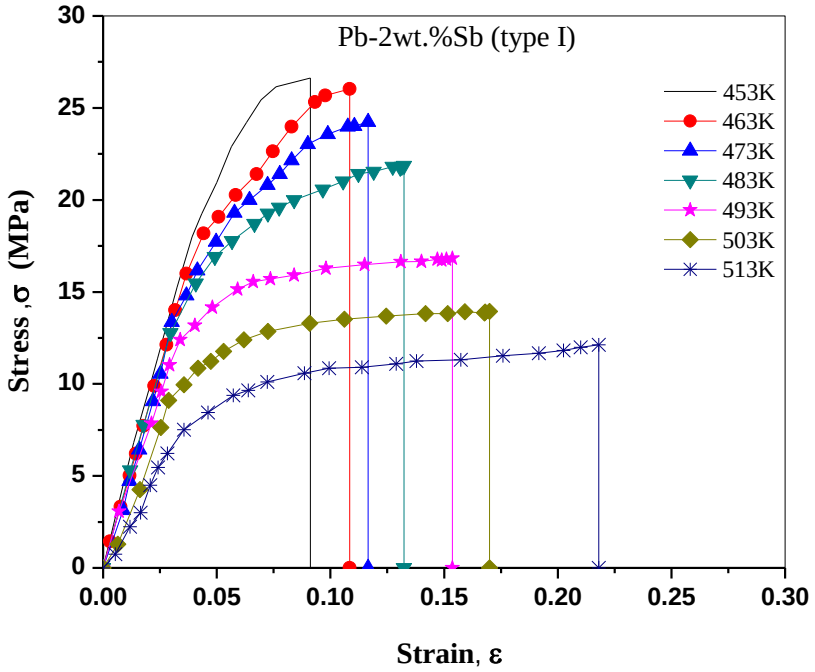

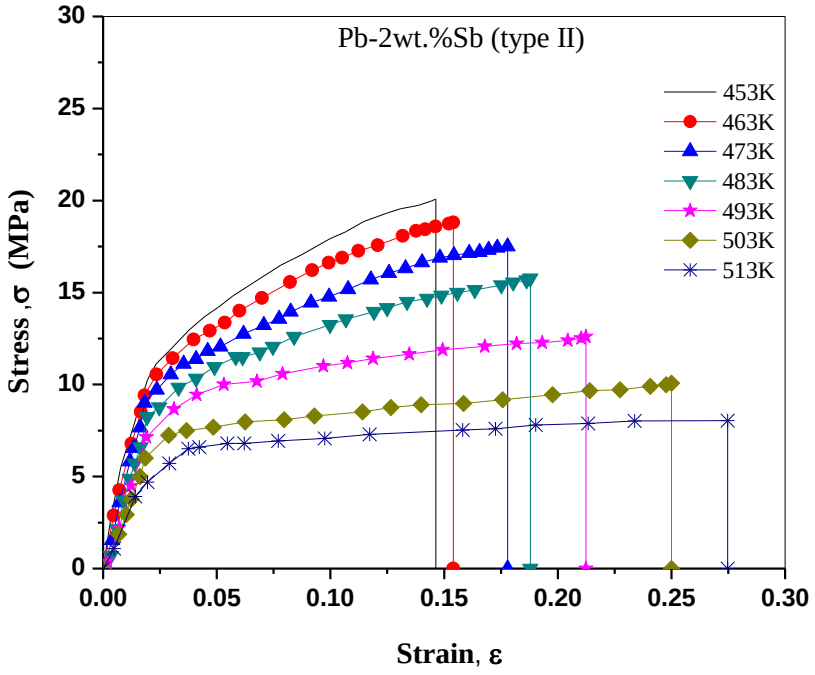

Fig. (2): Stress–strain curves of both types of Pb–2*wt*% Sb alloy.

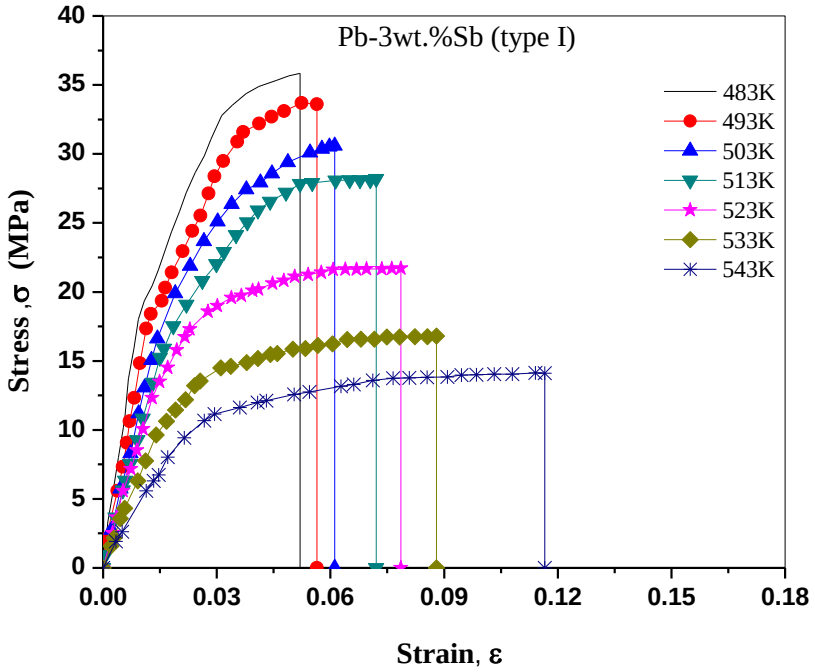

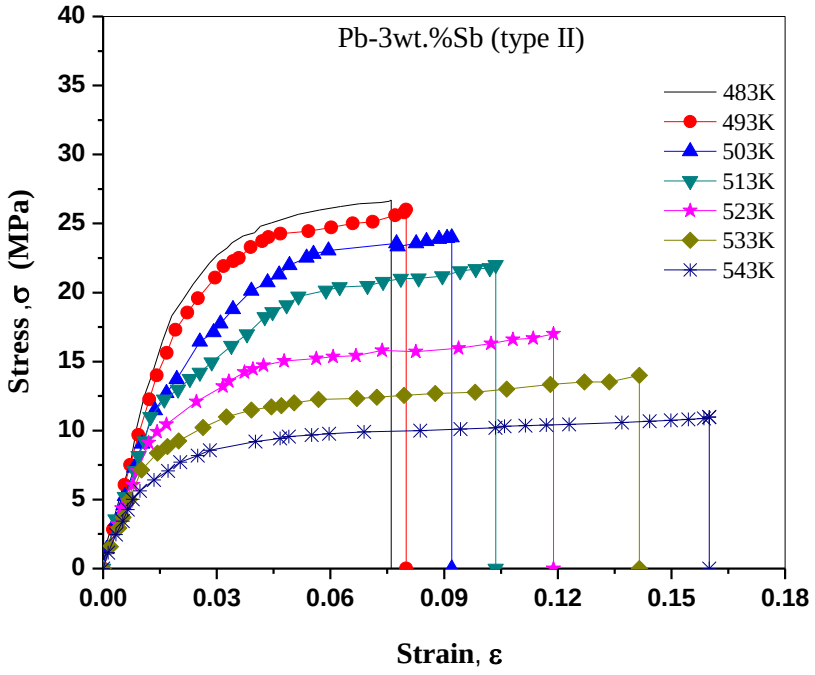

Fig. (3): Stress–strain curves of both types of Pb–3*wt*% Sb alloy.

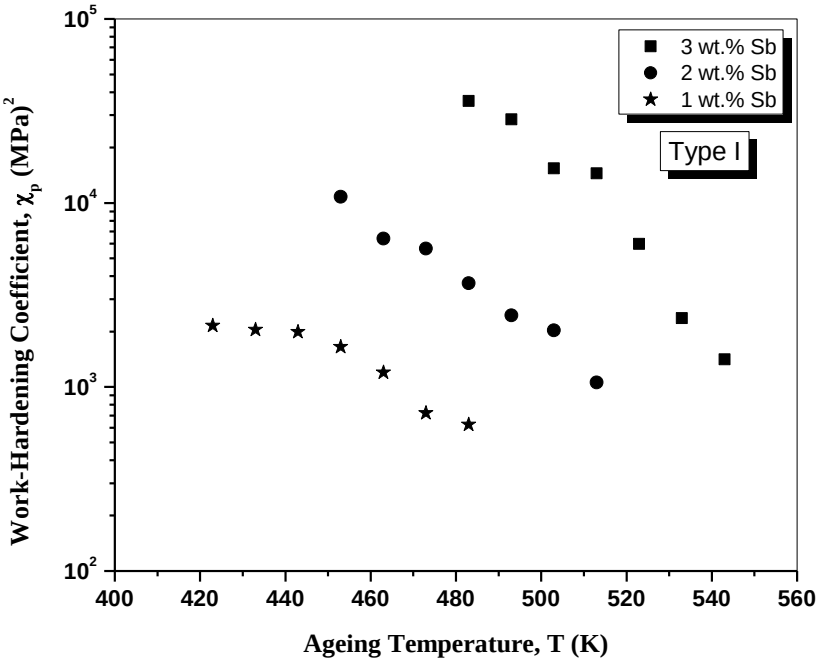

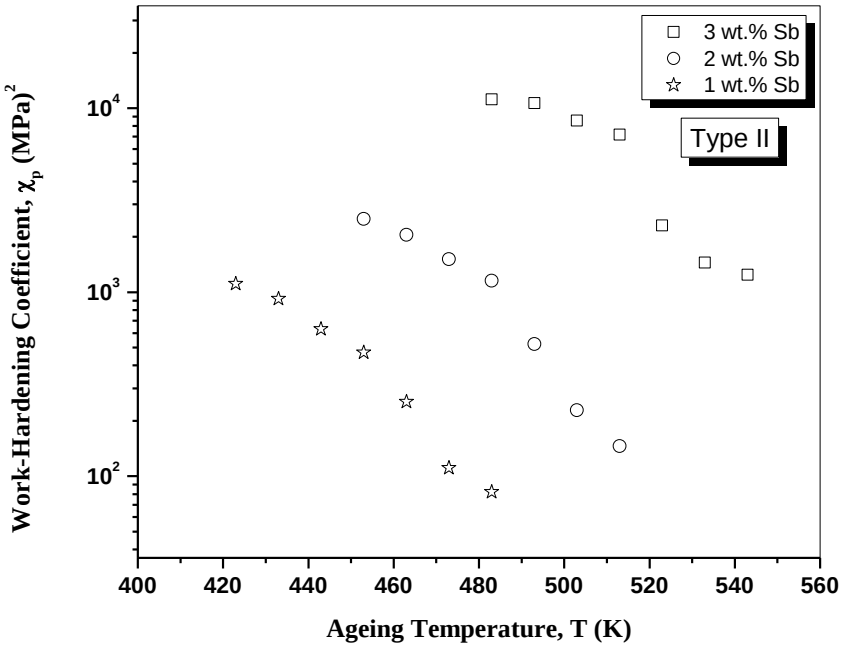

Fig. (4): The dependence of work-hardening coefficient, χ_p on the ageing temperature for both types of Pb–1-3*wt*% Sb alloys.

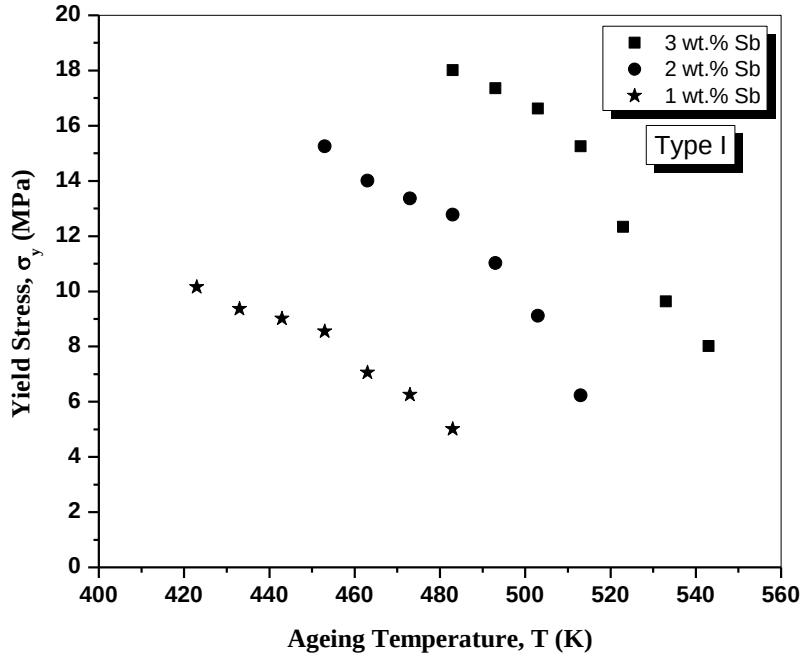

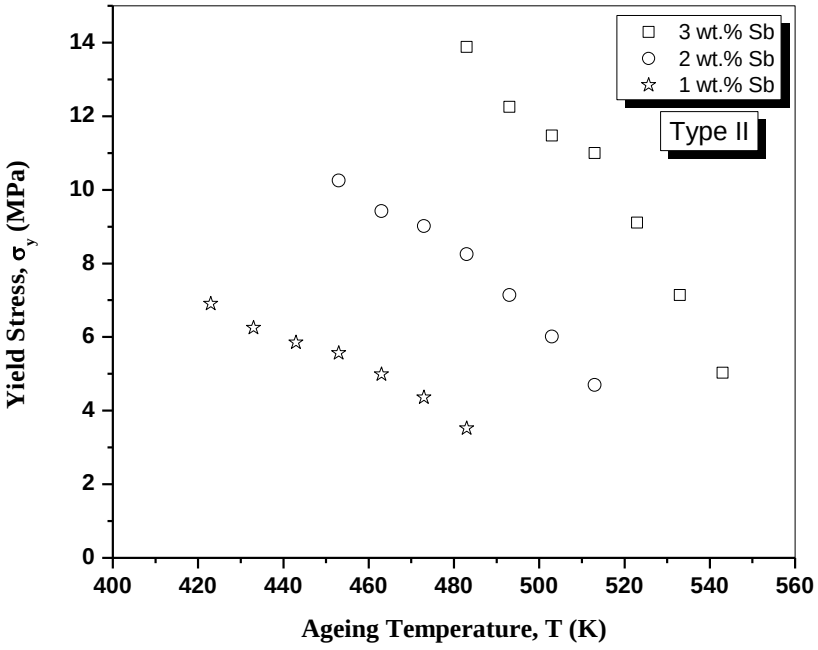

Fig. (5): The dependence of yield stress, σ_y on the ageing temperature for both types of Pb–1-3*wt*% Sb alloys

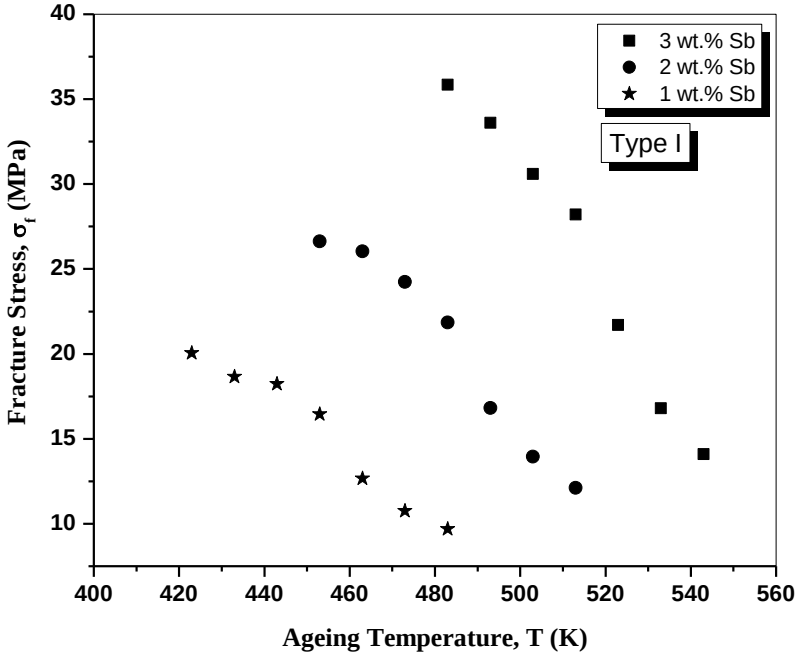

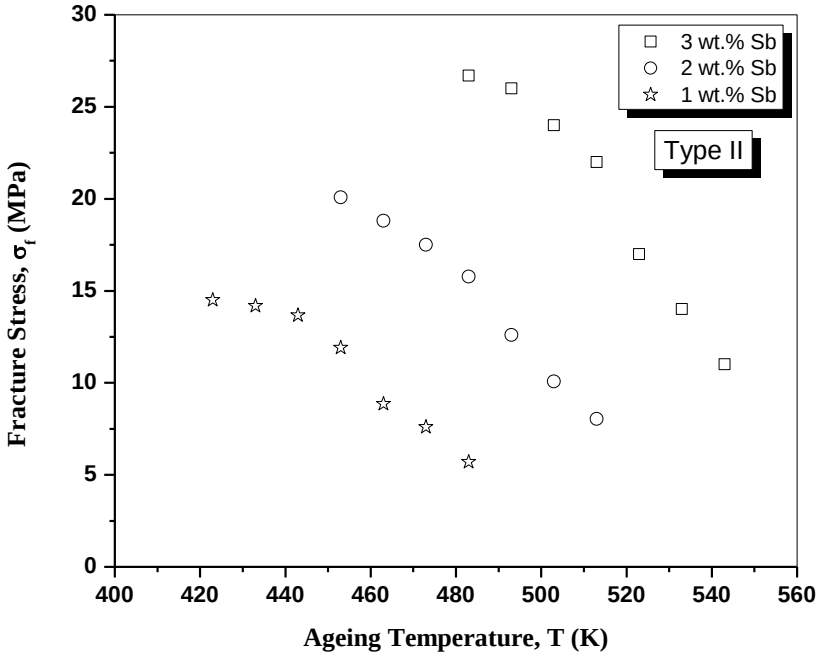

Fig. (6): The fracture stress, σ_f as a function of ageing temperature for both types of Pb–1-3*wt*% Sb alloys

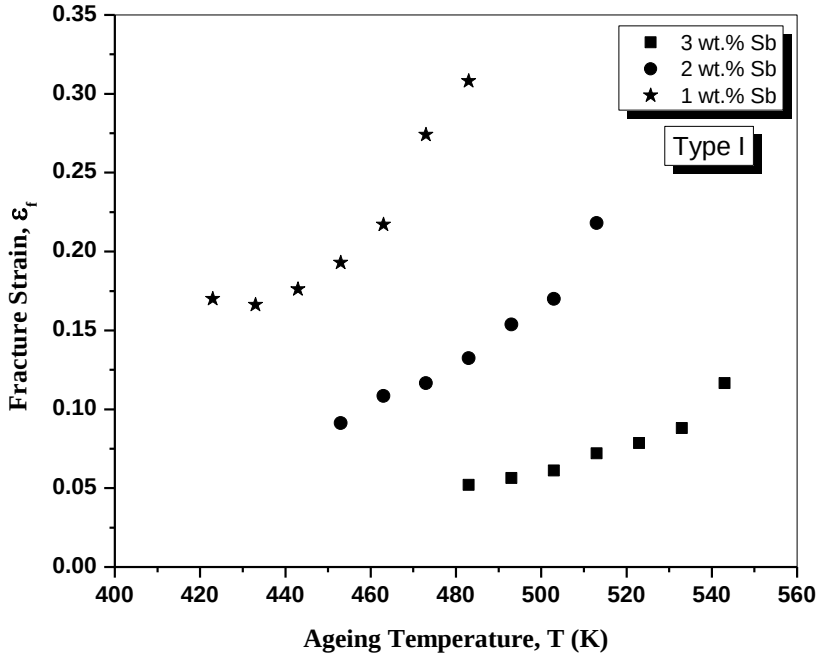

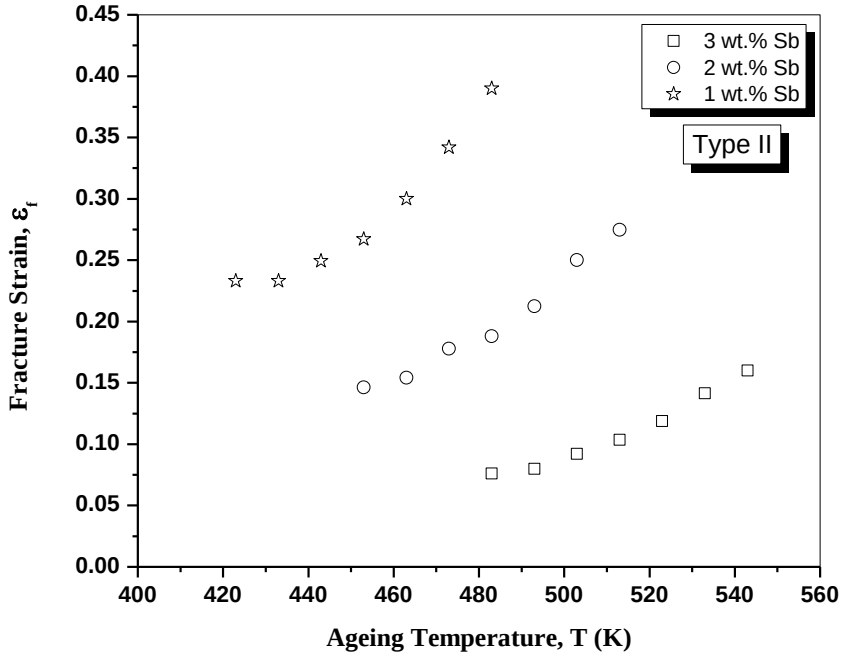

Fig. (7): The fracture strain, ε_f as a function of ageing temperature for both types of Pb–1-3*wt*% Sb alloys

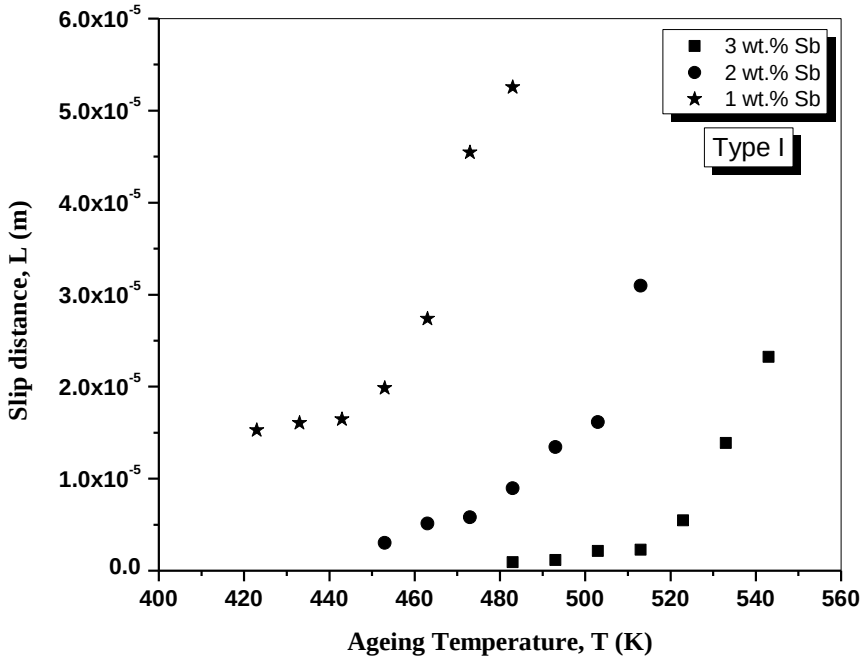

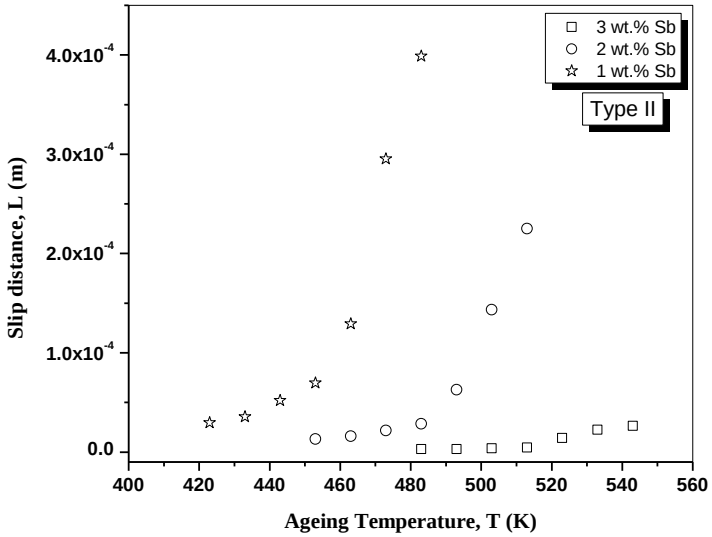

Fig. (8): Temperature dependence of slip distance, *L* for both types of Pb–1-3*wt*% Sb alloys

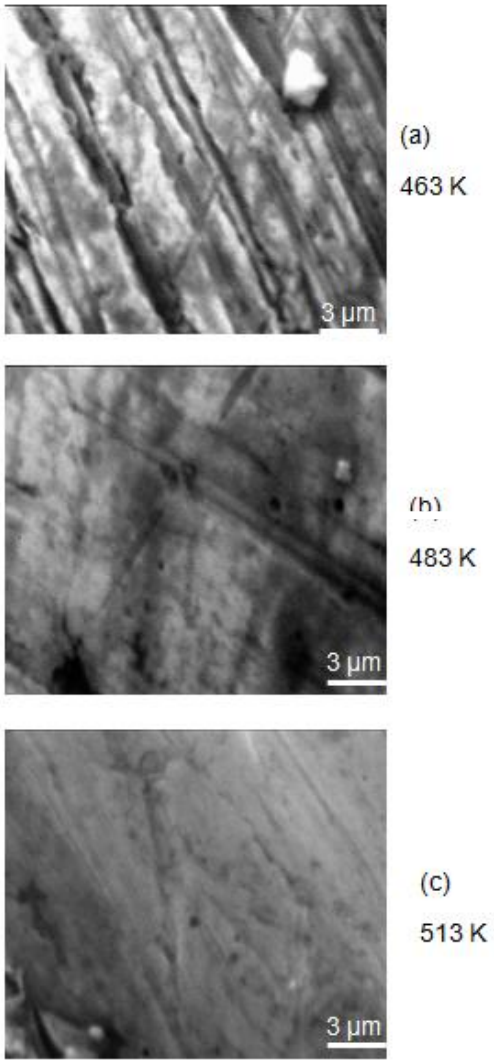

Fig. (9): SEM micrographs of the quenched samples (2*wt*.% Sb) at different ageing temperatures.

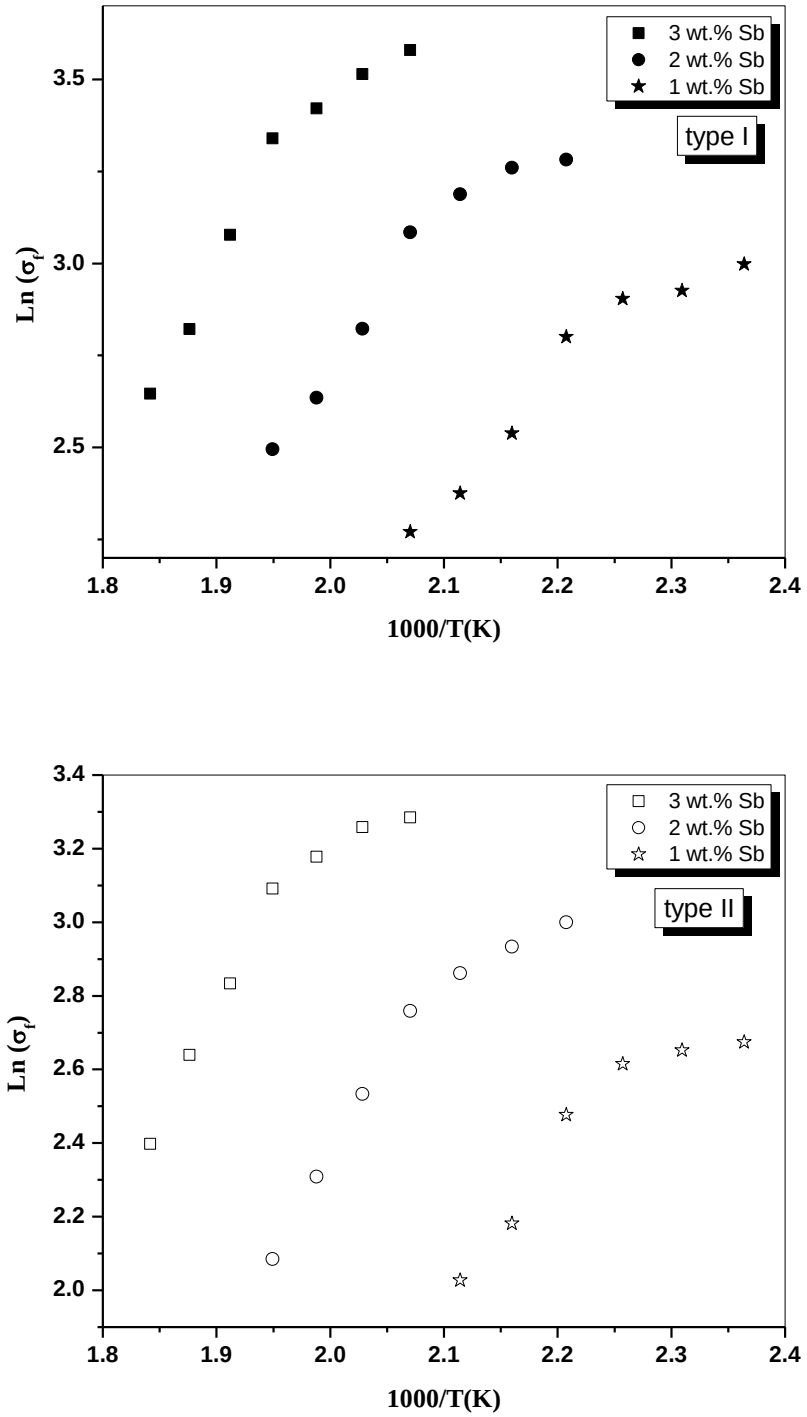

Fig. (10): The relation between Ln (σ_f) and 1000/T of both types of Pb–1-3*wt*% Sb alloys.